Volume determination of the Selo landslide complex (SW Slovenia): integrating field mapping, ground penetrating radar and GIS approaches

Timotej Verbovšek, Adrijan Košir, Maša Teran, Marjana Zajc & Tomislav Popit

Landslides
Journal of the International Consortium on Landslides

ISSN 1612-510X
Volume 14
Number 3

Landslides (2017) 14:1265-1274
DOI 10.1007/s10346-017-0815-x

Springer

Landslides (2017) 14:1265–1274
DOI 10.1007/s10346-017-0815-x
Received: 24 October 2016
Accepted: 23 February 2017
Published online: 14 March 2017

Timotej Verbovšek · Adrijan Košir · Maša Teran · Marjana Zajc · Tomislav Popit

Volume determination of the Selo landslide complex (SW Slovenia): integrating field mapping, ground penetrating radar and GIS approaches

Abstract The Selo landslide complex in the Vipava Valley (SW Slovenia) is a large fan-shaped sedimentary body that differs significantly from other slope deposits in the area in its exceptional size and considerable runout length. The landslide is predominantly composed of carbonate gravel deposited on a flysch paleo-relief. To determine the volume and geometry of the landslide and its potential source area, we integrated geological mapping, ground penetrating radar (GPR) and GIS techniques. The landslide deposits cover an area of about 10 km^2 with an average thickness of 10 m (maximum thickness reaching 56 m) and a maximum length of 5500 m. The volume of carbonate gravel was estimated from geological cross sections and GPR profiles. The base and top surfaces were interpolated by inverse distance and kriging methods, for which the Cut/Fill method was used in ESRI ArcGIS to determine the original landslide volume before the erosion. The estimated original volume is 190×10^6 m^3. The recent volume after the erosion is 96×10^6 m^3. The calculated volume of the Selo landslide, angle of reach $\theta = 10°$ and H/L ratio of 0.18 are in accordance with data for landslides of a comparable size. The most reasonable explanation for the development of the Selo landslide complex is a slope collapse involving the breakdown of the rock mass and the development of a high-mobility rock avalanche.

Keywords Rock avalanche · Long runout · GPR · Volume calculation · GIS · Slovenia

Introduction

The northern slopes of the Vipava Valley are one of the areas in Slovenia with the highest landslide susceptibility (Komac and Ribičič 2006). The geomorphology of the area is chiefly determined by a fold-and-thrust structure composed of a series of nappes of Mesozoic carbonates thrust over Paleogene flysch domains (Buser 1973; Placer et al. 2008). This structural and lithological setting exerts a primary control on the slope morphology, generally characterised by escarpment profiles with steep upper slopes in stronger, although highly fractured, carbonate rocks underlain by weaker shales, marls and sandstones, forming gentle lower slopes (Popit et al. 2014).

Extensive research over the last 15 years has focused on identifying triggering mechanisms and mitigating active landslides in the flysch of the Vipava Valley (Kočevar and Ribičič 2002; Mikoš et al. 2004; Logar et al. 2005; Fifer Bizjak and Zupančič 2009; Petkovšek et al. 2011; Popit and Verbovšek 2013), particularly in densely populated areas and along the construction route of the new motorway (Petkovšek et al. 2013; Mikoš et al. 2014). Aspects rarely addressed in previous research are the dynamics of the geomorphic slope system in the Vipava Valley through the late Quaternary, the identification of landslides, their extent, depositional history and potential triggering mechanisms.

We present a volumetric and geometric analysis of a large landslide complex, known as the Selo landslide (Popit and Košir 2003). This landslide complex differs from slope deposits and active landslides in the area in its exceptional size and considerable runout length, which is indicative of a rare, high-magnitude rock avalanche event. The main objective of this paper is to determine the volume and geometry of the landslide and its potential source area by integrating geological mapping, ground penetrating radar (GPR) and GIS techniques. The results are discussed in the context of estimating the material balance of the source area and the main landslide body.

Geological setting

The Selo landslide complex is located in the central part of the Vipava Valley in SW Slovenia (Fig. 1). The NE part of the valley is characterised by a high relief, extending from 50 to 200 m a.s.l. at the bottom of the valley to more than 1200 m a.s.l. on the edge of the high karst plateaus of the Trnovski Gozd and Nanos Mountains (Fig. 1). The relief is largely controlled by the Trnovo and Hrušica nappes, composed of Mesozoic, generally shallow-marine limestone and dolomite thrust over Paleocene and Eocene basinal deposits (flysch) composed of an alternation of sandstone, shale and marl (Fig. 1a). The flysch deposits are strongly folded, especially between the major thrust faults, while the carbonate rocks are intensively fractured along the thrust contacts and within wide zones of NW–SE trending strike-slip faults (Čar and Gospodarič 1988; Janež et al. 1997).

The slope morphology is primarily influenced by the difference in lithology of the thrust units and is characterised by steep cliffs in carbonates and gentle lower slopes formed in the underlying flysch. Most of the slopes are veneered by carbonate scree deposits (Fig. 1b), which locally reach several tens of metres in thickness (Buser 1973; Čar and Gospodarič 1988). The Trnovo Nappe in the broader area of the Selo landslide consists of Jurassic oolitic limestone, reef limestone and dolomite.

The Selo landslide (Fig. 1) covers an area of 10 km^2, with a top elevation of scarp between 1190 m a.s.l. (Mt. Čaven) and 1237 m a.s.l. (Mt. Veliki Rob) and a toe elevation of approximately 200 m a.s.l. (Popit and Košir 2003). The elevation difference (H) between the crest of the potential source area and the toe of the deposit is approximately 1000 m, while the length of the horizontal projection of the streamline connecting the extreme points of the landslide source and deposit (L) is 5500 m.

The upper part, the hinterland of sedimentary bodies of the Selo landslide in the cliff face of the Trnovski Gozd, is characterised by a pronounced arc-shaped structure that probably represents the main scarp (surface of a rupture with the crown at the top of the wall). Under the surface of the rupture are scree deposits, which overlap the contact with the main sedimentary body of the landslide. In the central part of its body, two streams have deeply cut into the carbonate deposits as well as into the flysch basement (Fig. 2). The larger and deeper Ravenščak Stream

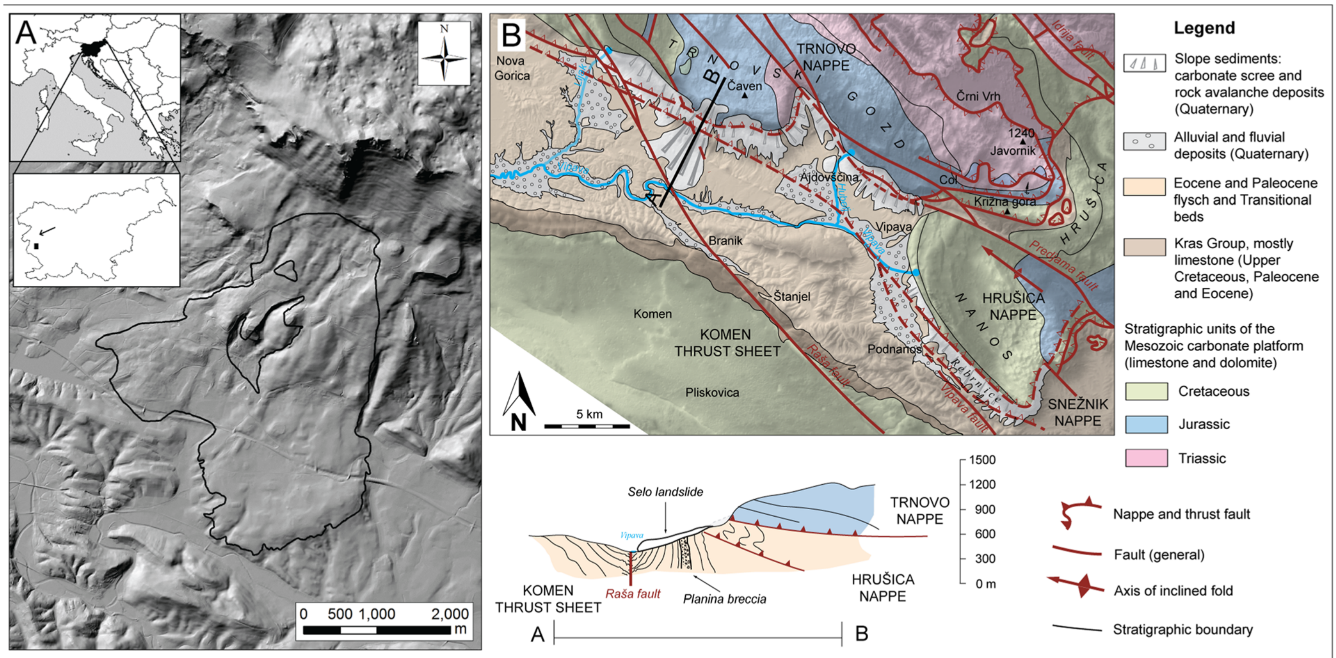

Fig. 1 **a** Location and extent of the Selo landslide. **b** Geological map of the broader area of SW Slovenia, with a cross section through the Selo landslide

is located on the NW side of the body, while the small Podstrel Stream is located on the SE side of the Tabor Hill (a flysch outcrop in the middle part of the sedimentary body). The sedimentary body borders the Vogršček Stream on the western side, while the eastern side is limited by the Gojače Stream, which is in contact with the sedimentary body of the carbonate slope deposit and flysch base rock. The lower part represents a fan-shaped sedimentary body, which is deposited on the flat bottom of the Vipava Valley and stretches all the way to the Vipava River.

The stratigraphy of the distal part of the landslide was well exposed in extensive road-cuts during motorway construction works near the village of Selo (Fig. 3a). In general, two facies units can be distinguished in the sedimentary body, deposited on paleo-relief, which is marked by a prominent palaeosol (PS): a lower, mud-supported unit (MS) and an overlying carbonate gravel unit (GS). The MS unit is up to 8 m thick and composed of pebbles, cobbles and several cubic metre blocks of limestone and sandstone, embedded in a muddy matrix. The sediment contains large tree trunks and a great quantity of wood debris. The structure of the sediment is chaotic. Large blocks occur in the upper part of the deposit. The GS unit is clast-supported and predominantly consists of limestone gravel with a subordinate amount of limestone cobbles and blocks. The gravel is poorly sorted and rarely exhibits an indistinctive imbrication of clasts (Popit 2003; Popit and Košir 2003). In the central and upper part of the landslide body, the GS unit lies directly on the flysch paleo-surface.

Radiocarbon dating of wood from the stump of a pine tree, rooted in the palaeosol, showed that the wood was older than 42 ka (quoted as a "radiocarbon-dead" sample; Popit and Košir 2003), indicating a Late Pleistocene (or older) age of the main landslide event.

Methods and equipment

To determine the volume, three methods were used: field mapping, GPR and ESRI ArcGIS software (ESRI 2012) for integrating the data, computing the volume and spatial analysis.

Field mapping

Mapping (basemap scale of 1:5000) was performed in the spring and summer of 2012, with the aim to determine the sedimentary facies and estimate the thickness of the GS unit. Such measurements were only possible in the upper and central parts of the landslide, where three ravines (visible in the digital elevation model (DEM) in Fig. 1b) were incised in the avalanche body: the Ravenščak ravine (22 locations), the Podstrel ravine (18 locations) and in the Vogršček ravine (7 measurements) (Fig. 2). Thickness was measured manually with a 30 m long measuring tape, with centimetre precision. In some places, for sediment thicknesses greater than 30 m, a marked rope was used for measurements. Point measurements were assigned with WGS84 spatial coordinates to be later used in the GIS environment.

Ground-penetrating radar

GPR has been successfully applied in several landslide research studies (Barnhardt and Kayen 2000; Bichler et al. 2004; Sass et al. 2008; Mantovani et al. 2013; Kadioglu and Ulugergerli 2012). In our study, GPR was used to determine the bedding plane of the GS unit of the landslide, which overlies the flysch paleo-surface or the MS unit. One should note that the MS unit has similar electromagnetic properties to those of the underlying flysch bedrock (composed of thin-bedded shale, marl and sandstone), so our study focused on the determination of the GS/MS or GS/flysch boundary, and not of the MS/flysch boundary. Also, the MS unit appears only in the southernmost (distal fan-shaped) part of the landslide.

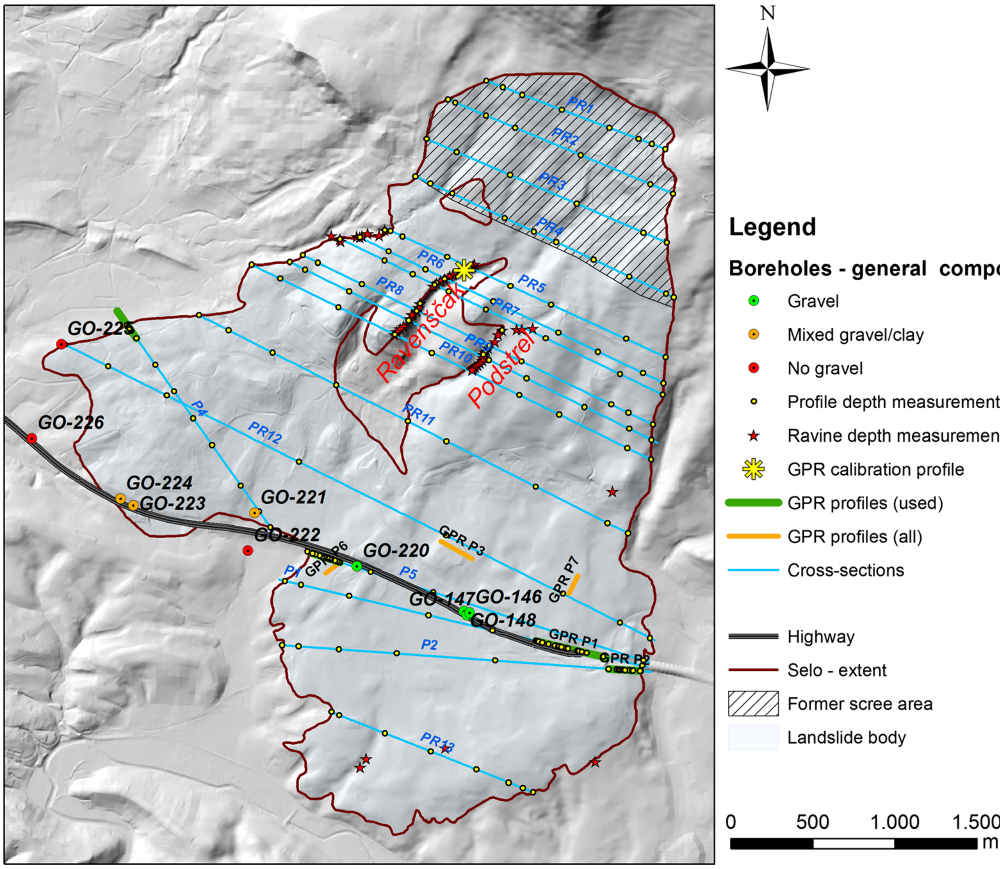

Fig. 2 Locations of the sediment thickness measurements in the ravines, GPR profiles, cross sections, boreholes and extent of the Selo landslide. Topographic names are taken from the state topological map with a scale of 1:25,000 from the Surveying and Mapping Authority of the Republic of Slovenia

For the purpose of this study, we used the Malå Geoscience ProEx GPR unit with an unshielded 50 MHz rough terrain antenna (RTA). The length of the antenna is 9.25 m, and the distance between the transmitter and receiver is 4 m (MALÅ Geoscience

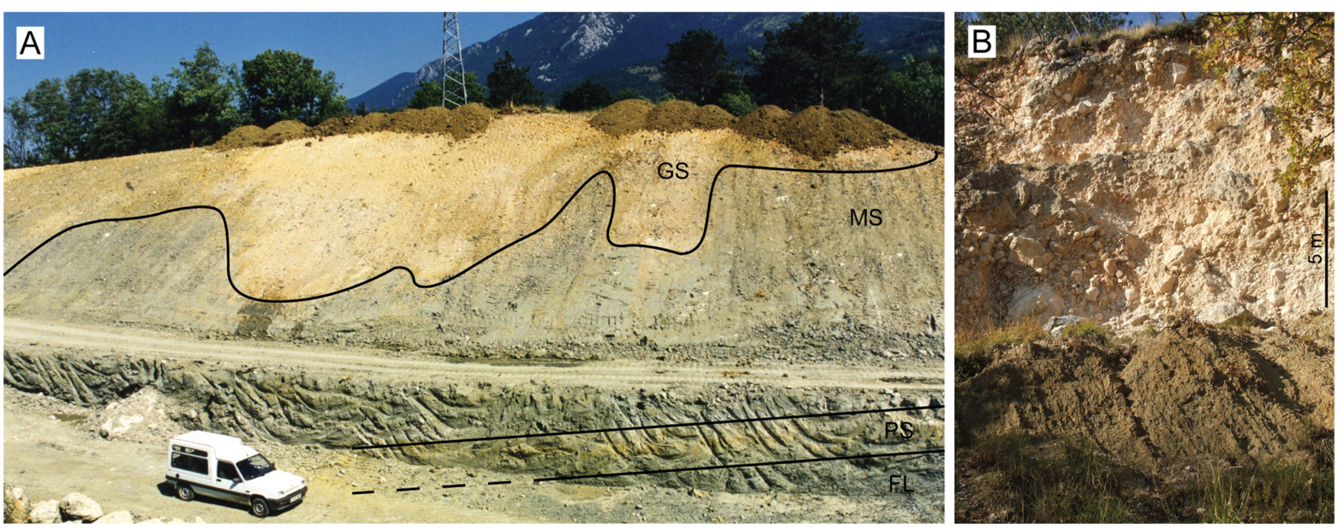

Fig. 3 **a** Location of GPR1 profile. Cross section of the Selo landslide on the Vipava-Nova Gorica motorway construction site in 1999. GS indicates that clast-supported unit consists predominantly of limestone gravel with a subordinate amount of limestone cobbles and blocks; MS indicates that a mud-supported unit composed of pebbles, cobbles and several cubic metre blocks of limestone and sandstone, embedded in a muddy matrix. *PS* palaeosol, *FL* flysch composed of an alternation of siltstone, sandstone and marls. **b** GS unit overlying the flysch in the Ravenščak ravine

2009). Despite the ability of the RTA to follow the relief, profile locations were mostly positioned in non-populated areas with uniform flat relief and measured along straight lines. GPR was mostly used in the lower part of the landslide where the GS unit was expected to be thinner.

The measurements were performed during a dry period to eliminate signal attenuation caused by the moisture of the sediment. Artificial objects, such as large metal objects, fences and electrical wires, and changes in elevation were marked on the GPR profiles during recording. The start and end points of the profiles were measured using a portable GPS receiver, and the coordinates were later used to calculate the profile lengths.

Seven GPR profiles were recorded in the lower part of the landslide (Fig. 2 and4): five parallel to the transport direction (439 long GPR P1, 193 m long GPR P2, 219 m long GPR P3, 204 m long GPR P4 and 177 m long GPR P5) and two perpendicular to the transport direction (100 m long GPR P6 and 120 m long GPR P7). Since the antenna used was unshielded, the latter two profiles contained too much noise from the surrounding area to determine the lower boundary of the carbonate sediment. Further, it was later discovered that the sediment of the GPR P3 profile location had been artificially replaced; hence, only four of the seven GPR profiles (P1, P2, P4 and P5) were used in the GIS analyses.

In order to convert the two-way travel time into depth, we need information about the velocity at which the signals are propagating through the material. However, no diffraction hyperbolas that are needed for the analysis of signal velocity could be defined in the recorded GPR profiles. Therefore, a depth calibration profile (CP, Fig. 4) was recorded parallel to a ravine, where the depth to the GS-MS boundary was measured in two points in the field. After defining this boundary in the depth calibration profile, the signal velocity of 0.128 m/ns was determined. This is the signal velocity at which the boundary depth matches the measured depth in the two field points. It corresponds to the material dielectric constant $\varepsilon = 5.5$, which is in accordance with the parameters established for these types of sediments. The dielectric constant for unsaturated sand and gravel spans from 3.5 to 6.5 (Neal 2004), for dry sand from 2 to 6 (Daniels 2004) and is defined at 5.5 for gravel (Saarenketo 2006).

The GPR data were analysed with the Sandmeier ReflexW Version 6.0.5 software. In order to remove the noise and improve the visibility of the stratigraphic boundaries, the following processing steps were applied: DC shift, time zero correction, background removal, manual gain (y) and bandpass filtering. Lastly, time was converted to depth using the depth calibration process, where the derived signal velocity was applied to all GPR profiles. Thus, the depth to the GS-MS boundary was accurately defined.

As a result, a depth profile was obtained for each cross section of the landslide body. The depth from the surface to the contact between the carbonate sediment and the underlying MS unit or flysch was then manually obtained from several points along each GPR profile. These data were later imported into GIS.

GIS determination of the bounding surfaces and volume calculation of the landslide

ESRI ArcGIS version 10.0 (ESRI 2012) was used to present digital maps and determine the landslide volume. Several approaches were combined in the GIS environment.

Organisation of the obtained data was undertaken within a relational spatial database. The extent of Selo was taken from the study by Popit and Košir (2003). A topographic base map was obtained using a DEM with a cell size of 5 × 5 m (DEM5) from 2006, which was provided by the Geodetic Survey of Slovenia. The field measurement data and GPR results were stored into two vector (feature class) point layers, storing the depth of contact and location of the points in the field.

Interpolation of the lower and upper bounding surfaces of the GS unit

The lower boundary of the GS unit ("basement surface," $S_B{}^{IDW}$ and $S_B{}^{KR}$) was interpolated from three map layers: the field measurements of sediment thickness, GPR data point depths and by assuming the thickness on the outer extent of the landslide to be zero. To interpolate this surface, two geostatistical methods were used for comparison: the inverse distance method (IDW) and kriging. In IDW, the points are weighted by the distance from an unknown (interpolated) point to known data points. This is a fast method and requires fewer parameters, although it can produce a "bull's eye" effect at some isolated points. Kriging is a much more sophisticated method for interpolation and is based on the geostatistical properties of the data (Swan and Sandilands 1995).

For the upper bounding surface of the GS unit, the surface was separated into the "recent" surface and "paleo-surface" of the carbonate gravel landslide before erosion. For the recent surface, we used the interpolation of DEM5 ($S_R{}^{DEM}$). For the reconstructed paleo-surface ($S_P{}^{IDW}$ and $S_P{}^{KR}$), 17 cross sections were drawn on the landslide body (Fig. 2) perpendicular to the transport direction. Four of these cross sections were in the direction of the GPR profiles (P1, P2, P4 and P5), and the others were perpendicular to the transport direction (PR1 to PR13). The ArcGIS Interpolate 3D Line tool was used to produce the elevation profile, and along this profile, the paleo-surface was drawn manually in such a way that the surface would most correctly represent the former carbonate gravel landslide and cover the recently eroded valleys. Data were then digitised in a similar way to the GPR profiles by measuring the carbonate sediment thickness from the basement surface to the reconstructed landslide paleo-surface at several points along the cross section.

Volume calculation

Volume was calculated as the difference between the two surfaces of the GS unit using the Cut/Fill method in ArcGIS (ESRI 2012). The method uses raster values in each cell and compares their heights, and the volume difference is expressed as positive if material was cut or negative if the material was added (filled). Such calculations were performed for both the IDW (IDW superscript in the following equations) and kriging methods (KR superscript):

1. Volume of recent landslide carbonate material:
   $V_R{}^{IDW} = \text{recent DEM surface } S_R{}^{DEM} - \text{basement surface } S_B{}^{IDW}$
   $V_R{}^{KR} = \text{recent DEM surface } S_R{}^{DEM} - \text{basement surface } S_B{}^{KR}$
2. Volume of the eroded part of the landslide:
   $V_E{}^{IDW} = \text{paleo-surface } S_P{}^{IDW} - \text{recent surface } S_R{}^{DEM}$
   $V_E{}^{KR} = \text{paleo-surface } S_P{}^{KR} - \text{recent surface } S_R{}^{DEM}$
3. Total volume of the landslide represents the sum of both recent and eroded material:

$$V_P{}^{IDW} = V_E{}^{IDW} + V_R{}^{IDW}$$

$$V_P{}^{KR} = V_E{}^{KR} + V_R{}^{KR}$$

Regarding the calculation of the potential source material, the missing volume of the scallops (visible on the DEM in Fig. 1 and

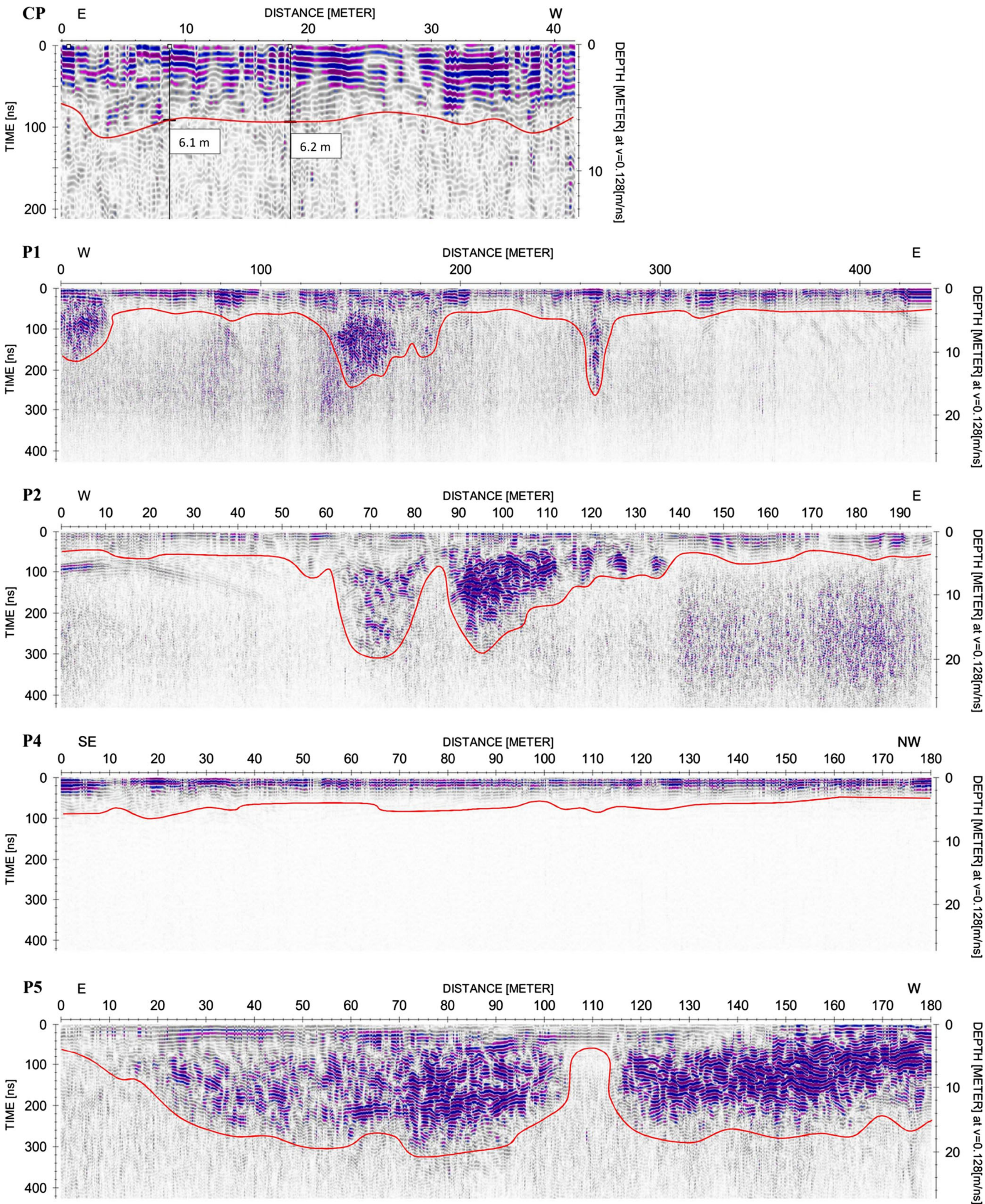

Fig. 4 GPR profiles CP, P1, P2, P4 and P5 with boundary marked between the GS and MS units. On the CP profile two points are marked, where the depth to the GS-MS boundary (6.1 and 6.2 m) was measured in the field

also as the blue shaded area in Fig. 5a) was estimated by contour modification. Contours (25-m vertical spacing) were drawn directly from the western to eastern ridges of the escarpment, thus reproducing the original surface above the recent relief and filling the volume. For the eastern "ridge," we used the surface slightly above the present terrain since modifying the contours directly to the present surface on the eastern side would not represent the actual continuous surface before mass transport. We modified the original surface for the main western arcuate scarps visible above the landslide. Sediment transported could have originated as rockfall from the bigger western scallop. After modifying the main scarp, a Triangulated Irregular Network (TIN) surface was produced from the contours (ArcGIS tool Create TIN). The volume was calculated using the Surface difference tool.

Results

Field measurements

The maximum measured thickness of the GS unit, up to 56 m, was obtained in the Ravenščak ravine (Fig. 3b). From 22 measurements, the thickness ranged from 1.5 to 56 m, and this greatest value was due to the central location of the ravine on the landslide body and the deepest incision. Five measurements did not reach the flysch basement or MS unit, and an indirect estimate of weathered material was used to determine the contact. In the Podstrel ravine, only two locations reached the flysch basement and were used in the study as the ravine was not eroded deeply enough everywhere to reach the flysch. The Vogršč"ek ravine has been deeply incised into the western side of the landslide. Three of nine points reached the flysch basement here, and the other six were used as an indirect estimate of the weathered material.

These measurements are supported by borehole data. The boreholes were drilled along the motorway (Andrić and Vavpotič 1987; Rijavec 1995; Fig. 2); however, they are only present along the southern part of the motorway. Several boreholes also did not reach the flysch basement and were unfortunately not useful for the calculation, although the gravel thickness is in agreement with the field studies. On the map (Fig. 2), the boreholes which encountered large quantities of gravel (GO-146, GO-147, GO-148 and GO-220) are marked in green. The first three were only drilled 10 m into the gravel, thus stopping inside the gravel layer. For the GO-220, only the last three metres (17 to 20 m) penetrated into the gravel, therefore also not reaching the boundary with flysch or MS unit. Some boreholes (GO-221, GO-223 and GO-224) were drilled through thin intercalations of clay, silt and gravel, and can be interpreted as MS/GS units, which also agrees with their position in the most distal part of the landslide. Boreholes outside the landslide area (GO-222, GO-225 and GO-226) did not encounter any gravel, only clay, silt or flysch basement.

GPR

Out of seven GPR profiles, four were used to determine the boundary between the GS and the MS layers. As seen in Fig. 4, a clear distinction between two different horizons can be made, although there is no pronounced reflector between the GS and MS layer. The reason that a strong reflector is not present in these GPR profiles is that the boundary lies between two different types of sediments and not between sediments and a layer of rock or even two layers of different rocks, which allow for strong reflections. In this case, the boundary is defined based on the behaviour of signals when passing through sediments with different electromagnetic properties. After travelling through the limestone gravel of the GS layer, the signals attenuate when they reach the highly lossy flysch bedrock or the mud-supported MS layer which has similar electromagnetic properties to those of the underlying flysch bedrock. We know from experience (Zajc et al. 2015) that GPR signals attenuate very rapidly when they reach flysch layers. The area where the signals attenuate to the point where no more reflections can be seen thus defines the boundary between the GS and the MS layer. Based on the boundary determined in the calibration profile, the shape of the mapped boundary in the ravine below the calibration profile and the shape of the boundary seen in the cross section of the motorway construction site (Fig. 3a), we conclude that the wavy attenuation boundary seen in the GPR profiles is the correct representation of the natural state. It should also be noted that the profiles have not been topographically calibrated; therefore, some of the unevenness of the boundary can also be the result of the uneven terrain. Several of these wavy contacts were observed in the lower part of the landslide (Fig. 4).

The theoretical minimum vertical GPR resolution depends on the antenna frequency and is defined at approximately one quarter of the GPR signal wavelength (Reynolds 1997; Neal 2004). The latter can be calculated by dividing the signal velocity in the given material with the value of the central antenna frequency. In our case, the 50 MHz antenna and 0.128 m/ns signal velocity within the gravel produce the signal wavelength of 2.56 m, a quarter of which gives a resolution of 0.64 m. This is theoretically the best resolution that can be achieved; however, in practice, the resolution is not as good (Reynolds 1997). This should be taken into consideration when interpreting GPR data recorded with low-frequency antennas. It should also be noted that converting the two-way travel time into depth can produce a ±10% error in determining the signal velocity values (Jol 2009). In our case, the signal velocity obtained from the calibration profile could therefore vary from 0.115 to 0.141 m/ns. After applying the two velocities to the GPR profiles, we found the difference in depth to be 1.5 m, which gives an error of ±0.75 m. In practice, an additional error could also be made when interpreting (drawing) the boundary in GPR profiles. The latter error is subjective (visual method) and not possible to quantify, and we estimate it could be overestimated in the range of 1 m or more, but not underestimated. Consequently, we have decided to apply the maximum possible ±10% error range to our calculations. This error is greater than the theoretical resolution error or subjective boundary depth determination error, and is less conservative compared to the two. Therefore, as the boundary GS/MS or GS/flysch, analysed by GPR, appears in the complete area of the landslide, we have applied this error range to all volume calculations, obtained from GPR measurements.

Regarding the comparison of GPR profiles with borehole data, the only borehole which lies close to the GPR profiles is GO-220. As mentioned above, it did not reach the flysch (or MS unit) basement and stopped at 20-m depth (Andrić and Vavpotič 1987). Also, the composition of first 17 m is not known (only the deeper profile). Comparison with the P5 GPR profile shows relatively good agreement, as the maximum thickness from the GPR profiles is approximately 20 m.

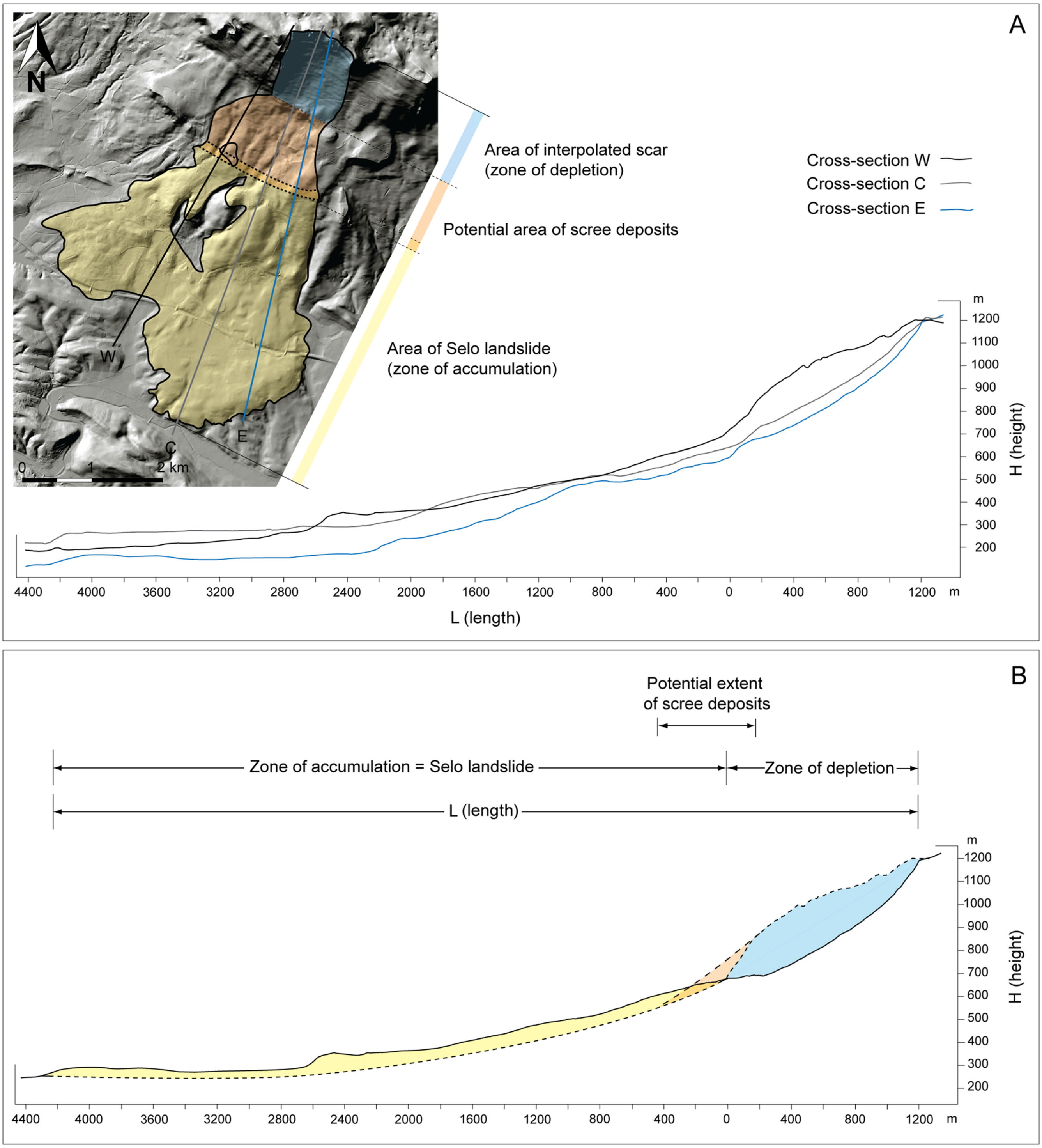

Fig. 5 **a** Extent of the Selo landslide and locations of the longitudinal cross sections W, C and E. **b** Longitudinal cross section of the Selo landslide at three zones (zone of depletion, potential extent of the talus slope and zone of accumulation)

Determination of the bounding surfaces and the volume calculation of the landslide in GIS

The lower surface was obtained by two interpolation methods, namely IDW and kriging, to obtain two different values for the calculation of the final landslide volume of the GS unit. It was interpolated to a grid of 5 × 5 m (same as the original DEM5 grid). The present surface is taken directly from DEM5 (Fig. 1a). From these three surfaces, two volumes were calculated. The volume before the erosion is calculated as the difference in elevation cells between the paleo-surface and the basement surface. The Cut/Fill method in ArcGIS produced a “positive” and “negative” volume, reflecting a positive gain in the cells (=deposition) and loss (=erosion). The calculated positive volume between the surfaces according to the kriging method was 201 × 10^6 m^3, and the negative volume was only 0.14 × 10^6 m^3 (V_P^{KR}). With the IDW method, the positive volume between the surfaces was 179 × 10^6 m^3 and the negative volume was 0.11 × 10^6 m^3 (V_P^{IDW}). The average of both methods (neglecting the very small negative volumes) therefore gives an estimate of the final landslide volume of 190 × 10^6 m^3. By applying the estimated ±10% range (±19 × 10^6 m^3) due to GPR measurement errors, the volume ranges from V_{min} = 171 × 10^6 m^3 to V_{max} = 209 × 10^6 m^3.

Regarding the average area of the landslide, the average thickness of landslide deposits is 19 m.

The volume of the eroded landslide volume was calculated as the difference between the paleo-surface and the DEM surface. The calculated volume using the kriging method was 91 × 10^6 m^3 and (V_E^{KR}). According to the IDW method, the eroded volume was 97 × 10^6 m^3 (V_E^{IDW}), giving an average of both methods of 94 × 10^6 m^3 (±9.4 × 10^6 m^3).

The recent volume was determined by the IDW method as 81 × 10^6 m^3 (V_R^{IDW}) and by kriging as 110 × 10^6 m^3 (V_R^{KR}), resulting in an average of 96 × 10^6 m^3 (±9.6 × 10^6 m^3). The average thickness of the recent sediment corresponds to about 10 m.

The calculated volume of the scallop is about 119 × 10^6 m^3. This value reflects the original carbonate source material in situ before dispersion due to the transport. As the initial volume of the original rock mass increases due to fragmentation and disintegration of the material (Hungr and Evans 2004), it is necessary to apply a volume-increase factor. We used a volume-increase factor of 25% (Hungr and Evans 2004) to correct this dispersion and obtained the volume of 1.25 × 119 × 10^6 m^3 = 149 × 10^6 m^3.

The last correction was to include the volume of scree deposited at the toe of the steep carbonate slope before the event. In the GIS environment, we drew the approximate extent of the scree (Fig. 2) according to the recent extent of scree deposits left on the western and eastern slopes of the Selo landslide, with the help of the DEM. The area covers about 1.4 km^2. By considering the average thickness of the scree to be about 10 m (Buser 1973; Janež et al. 1997), the volume of scree potentially incorporated by the landslide is 14 × 10^6 m^3.

By combining the calculated average volume from the scallops (149 × 10^6 m^3) and the volume of the scree (14 × 10^6 m^3), the final estimated volume of possible transported sediment amounts to about 163 × 10^6 m^3. Erosion of the flysch bedrock occurred during the transport, as flysch clasts can be found in the sediment body; however, the volume of incorporated flysch is negligible compared with the final sediment volume.

The final estimated volume of the landslide before erosion is 190 × 10^6 m^3 (±19 × 10^6 m^3, considering the error range due to GPR measurement errors), and the estimated volume of the sediment from the scallops and scree is 163 × 10^6 m^3. The difference between these values is in average about 16% and can be mostly attributed to the errors of the methods used, both in calculations of the volume before the erosion and also to the sensitivity of the surface interpolation due to the modification of the contours of the former relief.

Discussion

Geophysical methods (GPR) were useful in the lower parts of the landslide where no direct measurements could be made due to the predominance of flat areas without outcrops. As the depth of the contact between the carbonate sediment and the mud-supported sediment of flysch is only a few metres, it is probable that the sediment was either deposited on the paleo-surface of the former terrain or an older mud-flow deposit and/or the carbonate sediment has eroded the former flysch paleosurface or mud-flow deposit during transport. Such wavy contacts were clearly visible in the field (Fig. 3a) during construction of the H4 motorway in 1999, where the contact between the MS unit and the overlying GS unit is sharp but irregular (Popit 2003; Popit and Košir 2003).

The total volume of the displaced material is even larger given that, with the applied methods, only the volume of the GS unit was determined. However, the volume of mud-supported deposits (MS unit) is probably insignificant when the total landslide volume is considered.

Radiocarbon dating of the wood (Popit and Košir 2003) indicates the event age to be older than 42 ka. In the preliminary investigations, mostly based on the stratigraphy of the Selo landslide in the motorway sections, Popit and Košir (2003) speculated that the main body was formed by at least two separate flow events. However, the MS unit in the distal, marginal part of the landslide most probably indicates entrainment of the weathered flysch material along the flow path forming a lubricating layer (Hungr and Evans 2004). The long runout was most probably possible due to the self-generation of finer, weathered material (Hsü 1975). It is known that the movement of a large landslide mass is only possible in a narrow basal region in which energy is dissipated (Cleary and Campbell 1993) so that a large mass can be transported over a great distance.

This could be the case of the Selo landslide, as the landslide geometry is also consistent with the fragmentation-spreading model for dry granular avalanches developed by Davies and McSaveney (1999) and Davies et al. (1999). The estimated material balance, sediment volume and long runout geometry of this landslide complex shows that the main event might correspond to a large-scale slope collapse and development of a rock avalanche (Hsü 1975; Kilburn and Sørensen 1998; Hungr et al. 2001; McSaveney and Davies 2006; Hungr et al. 2014). This material entrapped the deposited carbonate scree and weathered flysch, and was transported far from its original source on the steep carbonate slopes.

The landslide volume alone is also a highly significant value since the runout distance depends primarily on the volume and less on the height of the (rock) fall (Legros 2002). The topography cross section (Fig. 5) shows a considerably long runout. The values of H (the elevation difference) and L (the length defined above) are H = 1000 m and L = 5500 m. This provides a H/L ratio of 0.18, corresponding to an apparent coefficient of friction and angle of reach (Fahrböschung of Heim 1932) θ = 10°.

There is a negative correlation between the apparent coefficient of friction (H/L) and the landslide volume (Straub 1997; Legros 2002). The volume and H/L value of the Selo landslide are in accordance with data for landslides of comparable size (Hsü 1975; Legros 2002), including some classical examples of subaerial non-volcanic landslides. Numerous landslides comparable in size and from similar geological settings formed as rock avalanches:

extremely rapid, massive flows of fragmented rocks generated by large rockfalls or slides. Hence, a slope collapse involving the breakdown of the rock mass and development of an avalanche of high mobility appears to be the most plausible explanation for the origin of the Selo landslide complex.

Such a conclusion raises the question as to whether such an event could occur in present times and poses a risk to people, buildings or infrastructure. For the analysed location around the Selo landslide, there is a low recurrence probability. However, the broader area is characterised by a similar geological setting with an intensive accumulation of carbonate scree, fractured steep slopes of carbonate nappes thrust over flysch and a relatively high seismic hazard (Živčič et al. 2000). Although the probability of a landslide event of such a magnitude is very low, the identification of other such events recorded in paleo-landslide deposits in the vicinity is therefore the first step in further research and is currently in progress.

Conclusions

The main findings may be summarised in the following points:

- Results of using a combination of field mapping, GPR profile measurements and GIS calculation methods show that the estimated volume of carbonate gravel before erosion was about 190×10^6 m^3 (±10% due to estimated GPR measurement errors). The combination of these methods was found to be successful for determining the volume of gravel deposits.
- The total volume of the displaced material is even larger given that only the volume of the carbonate gravel sediment was calculated and that a volume of entrained, mud-supported sediment remains in the lower part of the landslide.
- The estimated deposited (pre-erosional) volume of the landslide and the estimated rock volume from the scallops and scree (170×10^6 m^3) are very similar, indicating a probable genetic relationship of the landslide and scallop formation.
- The volume and angle of reach (or H/L value) of the Selo landslide complex are in accordance with data for landslides of a comparable size.
- The obtained results confirm that a slope collapse involving the breakdown of the rock mass and development of a high-mobility rock avalanche appears to be the most reasonable explanation for the origin of the Selo landslide complex.

Acknowledgements

The GPR survey within this study was conducted with the Ph.D. Grant 1000-10-310074 financed by the Slovenian Research Agency.

References

Andrić Z, Vavpotič K (1987) Engineering geological and geotechnical report on the conditions of the motorway Selo-Šempeter, from km 29.450 to km 41.600. Report number J-II-30d-a-15-414-n. Geological Survey of Slovenia, Ljubljana (In Slovene)

Barnhardt WA, Kayen RE (2000) Radar structure of earthquake-induced, coastal landslides in anchorage, Alaska. Environ Geosci 7:38–45. doi:10.1046/j.1526-0984.2000.71007.x

Bichler A, Bobrowsky P, Best M, Douma M, Hunter J, Calvert T, Burns R (2004) Three-dimensional mapping of a landslide using a multi-geophysical approach: the Quesnel forks landslide. Landslides 1:29–40. doi:10.1007/s10346-003-0008-7

Buser S (1973) Basic geological map of SFR Yugoslavia 1:100.000, Sheet Gorica L 33–78. Federal Geological Survey, Belgrade

Čar J, Gospodarič R (1988) Geološka zgradba in nekatere hidrološke značilnosti bruhalnika Lijaka = Geological setting and some hydrological properties of the Lijak effluent. Acta Carsol 17:13–32

Cleary PW, Campbell CS (1993) Self-lubrication for long runout landslides: examination by computer simulation. J Geophys Res 98:21911. doi:10.1029/93jb02380

Daniels DJ (2004) Ground penetrating radar. Institution of Electrical Engineers, London

Davies TR, McSaveney MJ (1999) Runout of dry granular avalanches. Can Geotech J 36:313–320. doi:10.1139/cgj-36-2-313

Davies TR, McSaveney MJ, Hodgson KA (1999) A fragmentation-spreading model for long-runout rock avalanches. Can Geotech J 36:1096–1110. doi:10.1139/t99-067

ESRI (2012) ArcGIS v.10. ESRI, Inc., Redlands, CA, USA

Fifer Bizjak K, Zupančič A (2009) Site and laboratory investigation of the Slano blato landslide. Eng Geol 105:171–185. doi:10.1016/j.enggeo.2009.01.006

Geoscience MALÅ (2009) ProEx – professional explorer control unit. Operating manual, Skolgatan

Heim A (1932) Bergsturz und Menschleben. Beiblatt zur Vierteljahrsschrift der Naturforschenden Gesellschaft in Zürich Geologische Nachlese No. 20, Jrg. 77: 218

Hsü KJ (1975) Catastrophic debris streams (sturzstroms) generated by rockfalls. Geol Soc Am Bull 86:129. doi:10.1130/0016-7606(1975)86<129:cdssgb>2.0.co;2

Hungr O, Evans SG (2004) Entrainment of debris in rock avalanches: an analysis of a long run-out mechanism. Geol Soc Am Bull 116:1240. doi:10.1130/b25362.1

Hungr O, Evans SG, Bovis MJ, Hutchinson JN (2001) A review of the classification of landslides of the flow type. Environ Eng Geosci 7:221–238. doi:10.2113/gseegeosci.7.3.221

Hungr O, Leroueil S, Picarelli L (2014) The Varnes classification of landslide types, an update. Landslides 11:167–194. doi:10.1007/s10346-013-0436-y

Janež J, Čar J, Habič P, Podobnik R (1997) Vodno bogastvo Visokega krasa : Ranljivost kraške podzemne vode Banjšic, Trnovskega gozda. Nanosa in Hrušice. Geologija d.o.o, Idrija

Jol HM (2009) Ground penetrating radar: theory and applications. Elsevier

Kadioglu S, Ulugergerli EU (2012) Imaging karstic cavities in transparent 3D volume of the GPR data set in Akkopru dam, Mugla, Turkey. Nondestruct Test Eva 27:263–271. doi:10.1080/10589759.2012.694885

Kilburn CRJ, Sørensen S-A (1998) Runout lengths of sturzstroms: the control of initial conditions and of fragment dynamics. J Geophys Res 103:17877. doi:10.1029/98jb01074

Kočevar M, Ribičič M (2002) Geološke, hidrogeološke in geomehanske raziskave plazu Slano blato = geological, hydrogeological and geomechanical investigation of the Slano blato landslide. Geologija 45:427–432

Komac M, Ribičič M (2006) Landslide susceptibility map of Slovenia at scale 1:250,000. Geologija 49:295–309. doi:10.5474/geologija.2006.022

Legros F (2002) The mobility of long-runout landslides. Eng Geol 63:301–331. doi:10.1016/s0013-7952(01)00090-4

Logar J, Bizjak KF, Kočevar M, Mikoš M, Ribičič M, Majes B (2005) History and present state of the Slano blato landslide. Nat Hazard Earth Sys 5:447–457

Mantovani M, Devoto S, Forte E, Mocnik A, Pasuto A, Piacentini D, Soldati M (2013) A multidisciplinary approach for rock spreading and block sliding investigation in the north-western coast of Malta. Landslides 10:611–622. doi:10.1007/s10346-012-0347-3

McSaveney MJ, Davies TRH (2006) Inferences from the morphology and internal structure of rockslides and rock avalanches rapid rock mass flow with dynamic fragmentation. In: Evans SG, Mugnozza GS, Strom A, Hermanns RL (eds) Landslides from massive rock slope failure. Springer Netherlands, Dordrecht, pp 285–304

Mikoš M, Četina M, Brilly M (2004) Hydrologic conditions responsible for triggering the Stoze landslide, Slovenia. Eng Geol 73:193–213. doi:10.1016/j.enggeo.2004.01.011

Mikoš M, Sodnik J, Petkovšek A, Maček M, Majes B (2014) WCoE: mechanisms of landslides in over-consolidated clays and flysch and IPL-151 project: soil matrix suction in active landslides in flysch—the Slano blato landslide case. In: Sassa K, Canuti P, Yin Y (eds) Landslide science for a safer Geoenvironment. Springer Netherlands, Dordrecht, pp 143–148

Neal A (2004) Ground-penetrating radar and its use in sedimentology: principles, problems and progress. Earth Sci Rev 66:3–4. doi:10.1016/j.earscirev.2004.01.004

Petkovšek A, Fazarinc R, Kočevar M, Maček M, Majes B, Mikoš M (2011) The Stogovce landslide in SW Slovenia triggered during the September 2010 extreme rainfall event. Landslides 8:499–506. doi:10.1007/s10346-011-0270-z

Petkovšek A, Maček M, Mikoš M, Majes B (2013) Mechanism of active landslides in flysch. In: Sassa K, Rouhban B, Briceño S, McSaveney M, He B (eds) Landslides: Global Risk Preparedness. Springer, Berlin, pp 149–165

Placer L, Jež J, Atanackov J (2008) Structural aspect of the Slano blato landslide (Slovenia). Geologija 51:229–234

Popit T (2003) Pleistocenski sedimenti blatno-drobirskih tokov pri Selu v Vipavski dolini. University of Ljubljana

Popit T, Košir A (2003) Pleistocene debris flow deposits in the Vipava Valley, SW Slovenia. In: Vlahović I (ed) 22nd IAS Meeting of Sedimentology Institute of geology, Zagreb, Opatija, Croatia, pp 161

Popit T, Verbovšek T (2013) Analysis of surface roughness in the Sveta Magdalena paleo-landslide in the Rebrnice area. RMZ - Mater and Geoenviron 60:197–204

Popit T, Rožic B, Šmuc A, Kokalj Ž, Verbovšek T, Košir A (2014) A lidar, GIS and basic spatial statistic application for the study of ravine and palaeo-ravine evolution in the upper Vipava valley, SW Slovenia. Geomorph 204:638–645. doi:10.1016/j.geomorph.2013.09.010

Reynolds JM (1997) An introduction to applied and engineering geophysics. Wiley, West Sussex, p 796

Rijavec, B. (1995) Final geotechnical report on the conditions of the foundation 5–9 on the km 30.444. AC Selo-Šempeter. Report number J-II-30d-a-15-414-n. Geological Survey of Slovenia, Ljubljana (In Slovene)

Saarenketo T (2006) Electrical properties of road materials and subgrade soils and the use of ground penetrating radar in traffic infrastructure surveys. Acta Universitatis Ouluensis A471

Sass O, Bell R, Glade T (2008) Comparison of GPR, 2D-resistivity and traditional techniques for the subsurface exploration of the Öschingen landslide, Swabian Alb (Germany). Geomorph 93:89–103. doi:10.1016/j.geomorph.2006.12.019

Straub S (1997) Predictability of long runout landslide motion: implications from granular flow mechanics. Geol Rundsch 86:415–425. doi:10.1007/s005310050150

Swan ARH, Sandilands M (1995) Introduction to geological data analysis. Blackwell Science, Oxford

Zajc M, Celarc B, Gosar A (2015) Structural-geological and karst feature investigations of the limestone-flysch thrust-fault contact using low-frequency ground penetrating radar (Adria-Dinarides thrust zone, SW Slovenia). Environ Earth Sci 73(12):8237–8249. doi:10.1007/s12665-014-3987-x

Živčič M, Suhadolc P, Vaccari F (2000) Seismic zoning of Slovenia based on deterministic hazard computations. Pure Appl Geophys 157:171–184

T. Verbovšek (✉) · T. Popit
Department of Geology,
University of Ljubljana, Faculty of Natural Sciences and Engineering,
Privoz 11, SI-1000, Ljubljana, Slovenia
e-mail: timotej.verbovsek@ntf.uni-lj.si

A. Košir
Ivan Rakovec Institute of Palaeontology,
Research Centre of the Slovenian Academy of Science and Arts,
Novi trg 2, SI-1000, Ljubljana, Slovenia

M. Teran
Savska cesta 13, SI-4270, Jesenice, Slovenia

M. Zajc
Faculty of Natural Sciences and Engineering, Department of Geotechnology, Mining and Environment,
University of Ljubljana,
Aškerčeva 12, SI-1000, Ljubljana, Slovenia

A. Košir
School of Earth and Ocean Sciences,
Cardiff University, Main Building, Park Place,
CF10 3AT, Cardiff, UK